

Flexible-die forming process with solid granule medium on sheet metal

Guo-jiang DONG¹, Chang-cai ZHAO¹, Miao-yan CAO²

1. Key Laboratory of Advanced Forging and Stamping Technology and Science,
Ministry of Education, Yanshan University, Qinhuangdao 066004, China;

2. National Engineering Research Center for Equipment and Technology of Cold Strip Rolling, Yanshan University,
Qinhuangdao 066004, China

Received 23 February 2013; accepted 10 April 2013

Abstract: Certain non-metallic granules (NMG) were selected as the research object. It was proposed to conduct the volume compression experiments as well as those on the NMG physical properties at high stress levels. Then, not only the volume compression ratio curve but also the extended Drucker-Prager linear model were obtained. In addition, through the friction strength tests, parameters of the Mohr-Coulomb model were gained, which proved in basic agreement with those of the extended Drucker-Prager linear model. Additionally, curves of the friction coefficients between the NMG and the sheet metal under different pressures were also obtained. Based on the material performance experiments, numerical analysis in respect of flexible-die forming process with solid granule medium (SGM) was conducted. The die and device for experiments of solid granule medium forming (SGMF) on sheet metal were designed and manufactured. Typical parabolic parts were successfully trial-produced. The tests and simulation results show that the sheet formability is significantly improved for the extraordinary friction performance during interaction between the SGM and the sheet metal surface. The process control and die structure are simple, and the shaped work-pieces enjoy many advantages, such as satisfactory surface quality and favorable die fitability, which offers a brand-new method and means for processing and preparation of sheet metals.

Key words: solid granules medium forming; drawing; sheet metal; finite element simulation

1 Introduction

Flexible-die forming on sheet metal employs a rigid female die (or punch) and specific pressure-transfer medium as the rigid punch (or female die), such as solid medium rubber and polyurethane, liquid water and oil, gaseous compressive air and viscous medium. The sheet metal is shaped under the effect of the pressure-transfer medium. Flexible-die forming technology on sheet metal, as an advanced and flexible forming method, has gained rapid development and wide application [1–3]. Recently, it has gradually become one of the mainstream manufacturing technologies for thin-walled parts. According to the process properties scholars from various countries have conducted relevant researches on aspects of theoretical analysis, experiment and numerical simulation. The main focuses are on parts with complex shape, extraordinary deep drawing limit and materials with low plasticity and formability. Satisfactory results have been achieved, and some of the technologies have

been successfully applied to aerospace, automotive manufacturing and other fields. Hydroforming deep drawing (HDD) and viscous pressure forming (VPF) are the same as the representatives of the flexible-die forming technology and have been developed rapidly [4–7].

HAMA et al [8] made an analysis on sheet hydroforming process of elliptical cup workpiece, using the static finite element software STAMP3D. They attested that in the process of hydrodynamic deep drawing, the friction between the male die and the sheet deformation can prevent the sheet's local shrinking, and that the board's drawing capacity can be improved. KHANDEPARKAR and LIEWALD [9] investigated the ability of transferring complex features from the punch onto the blank surface with high deep drawing ratios, and the extended limiting deep drawing ratios of 3.0 for the low-carbon (DC04) drawing part and 2.875 for the stainless (DIN 1.4301) drawing part had been achieved. LANG et al [10] simulated and tested the hydroforming of aluminum and stainless steel with complex surface

through the multi sheet hydroforming process, in which the measures of controlling forming quality were presented. WANG et al [11,12] proposed HDD with radially inward flowing liquid, to establish the limit drawing ratio and pressure ratio of the forming region, and an aluminum alloy 2A120 cup with a drawing ratio of 2.85 was obtained. Liquid soft die forming of sheet can be especially applied in the production of the workpieces with high requirements such as complex shape, high quality of appearance and the giant workpieces of panel. This technology can simplify the complex sheet metal production and provide the production with good flexibility, fine structures and less elasticity. However, deep drawing technology requires high pressure from liquid pressure system, practical cavity sealing plans and sophisticated liquid pressure system designs, leading to a higher production cost and more difficulties of the technology implementation.

Viscous medium has many characteristics, e. g., it is easy to seal, pressure is also easy to control, especially the adhesion between the sheet is good for homogenization of the plate. AHMETOGLU et al [6] applied VPF process to form non-symmetric part from steel, aluminum and nickel alloy, and studied how process parameters such as clamping load, forming speed, medium pressure and part geometry influence the formability through finite element simulations and experimental analysis. WANG and YI [7] got the forming limit curve of 6k21-T4 sheet through viscoelastic-plastic flexible-die bulging experiments. The outer door of car with scale-down simulating dimensions was chosen as experimental parts for panels, and the viscoelastic-plastic flexible-die forming experiments were carried out to analyze the effect of the relationship between viscoelastic-plastic flexible-die pressure and blanker holding force (BHF) on the formability of aluminum panels. LIU and WANG [13] formed the aluminum ladder part with VPF process, and the fracturing and flange wrinkling failures were predicted via the sectional finite element method simulation. Their study showed that the increase of interface friction force is helpful to restraining the flange wrinkling and local fracturing in VPF process. FU et al [14] conducted numerical study to look into the deformation behaviors of this process by explicit 3D-FE simulation under the ABAQUS platform. They conducted a comparison between the conventional deep drawing (CDD) and the viscoplastic pressure-carrying medium (VPCM) in terms of wall-thickness reduction, hydrostatic pressure, principal stress distribution and damage factor. Their simulation results show that the higher VPCM pressure could result in the higher hydrostatic pressure throughout the process and further resist wall thinning and prevent the fracture of the sheet metal. Scholars from various countries have

conducted a large number of viscous medium performance tests and viscous pressure forming process tests, and have fully proved the feasibility and advantage of the process, which laid a solid theoretical foundation for practical application of the process. However, heat resistance of the viscous medium limits its application areas.

ZHAO et al [15–17] proposed a brand-new flexible forming technology, using solid granule medium as the pressure-transfer medium, which is solid granule medium forming (SGMF). Metallic or non-metallic granules (abbreviation for MG or NMG), similarly spherical shape with diameters from $d0.05$ mm to $d2$ mm were selected as pressure-transfer medium to form the work-piece, with the process principle shown in Fig. 1.

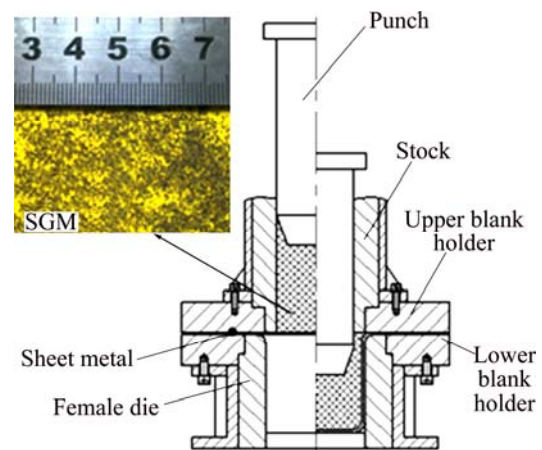


Fig. 1 Schematic diagram of SGMF on sheet metal

The significant feature different from the traditional soft-mold forming lies in the fact that the pressure-transfer medium is changed, therefore the forming law is distinctive. In this work, experiment on physical properties of solid granule medium at high stress levels is conducted, and based on this, the numerical analysis with respect to SGMF on sheet metal is conducted. The forming die and device are designed and manufactured. Typical parabolic parts are successfully trial-produced, which lays an experimental and theoretical basis for actual application of this technology.

2 Material performance test on solid granule medium

The SGM has a good flowability and only maintains its stacked shape within a certain range. It does not withstand tension; however, it can withstand substantial pressure and shear force, and the force bearing capacity enhances as the confining pressure increases. The discrete characteristic of the SGM determines its complex physical features and mechanical properties manifested during the loading and unloading processes.

Researches on physical properties of SGM under high pressures have a very important significance on in-depth exploration and practice of the SGMF technology.

The stress state of the granule system (GS) on one point is signified by the stress tensor σ_{ij} , which is decomposed into the spherical stress tensor σ_m with uniform stress in all directions and the deviatoric stress tensor s_{ij} , that is,

$$\sigma_{ij} = s_{ij} + \sigma_m \delta_{ij}, \delta_{ij} = \begin{cases} 0 & (i \neq j) \\ 1 & (i = j) \end{cases} \quad (1)$$

Yield surface is commonly defined by stress invariants in advanced soil mechanics [18], which provides that when the normal stress is pressure it is positive. As to the shear stress, the counterclockwise direction of its corresponding surface's outward normal is positive, namely,

1) Average principal stress p :

$$p = \sigma_{\text{oct}} = \frac{1}{3}(\sigma_1 + \sigma_2 + \sigma_3) = \sigma_m \quad (2)$$

2) Equivalent stress q :

$$q = \frac{1}{\sqrt{2}} [(\sigma_1 - \sigma_2)^2 + (\sigma_2 - \sigma_3)^2 + (\sigma_3 - \sigma_1)^2]^{\frac{1}{2}} \quad (3)$$

3) The third stress invariant r :

$$r = \frac{9}{2} (s_{ij} s_{jk} s_{ki})^{\frac{1}{3}} \quad (4)$$

In this work, NMG is selected as the research objects, wherein 3# NMG diameters are between 0.084–0.104 mm, 5# NMG diameters 0.117–0.14 mm, and 8# NMG diameters 0.221–0.318 mm. NMG belongs to the non-viscous materials, namely, the cohesion equals zero.

2.1 Volume compression test on SGM

The SGM is granular bodies, which exhibit in the hydrostatic stress state during the sheet forming process and produce certain volume compression during their coupling deformation phase with the sheet metal. When the stress state is $\sigma_1 > \sigma_2 = \sigma_3$, the stress invariants respectively turn out to be

$$p = (\sigma_1 + 2\sigma_3) / 3, \quad q = \sigma_1 - \sigma_3, \quad r = \sigma_3 - \sigma_1 \quad (5)$$

The testing device of volume compression for SGM was designed according to the stress state during the sheet forming process. The relation curves between the NMG average principal stress and the equivalent shear stress is displayed in Fig. 2.

Yield locus for NMG on the $p-q$ stress plane is precisely fitted by a linear equation, namely, the equivalent shear stress and the average principal stress exhibit a linear relationship (see Fig. 2(a)), which proves it is identical with the assumption of the extended Drucker-Prager linear model in advanced soil mechanics, that is,

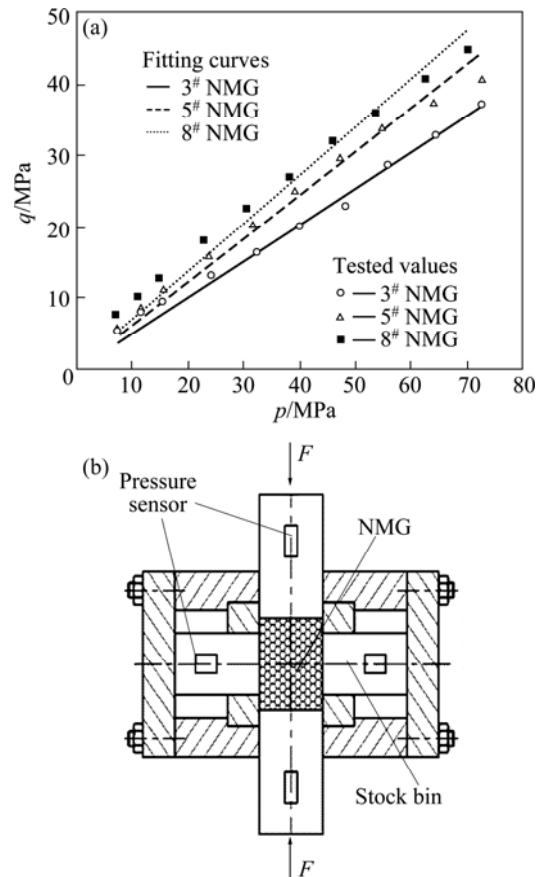


Fig. 2 Volume compression test on SGM: (a) $p-q$ stress curve of NMG; (b) Schematic diagram of SGM

$$F = t - p \tan \beta - d = 0 \quad (6)$$

where d denotes the material cohesion, i.e. $d=0$; β denotes the tilt angle of linear yield locus on $p-q$ stress plane, known as the Drucker-Prager friction angle; t stands for the deviatoric stress tensor parameter with respect to the roundness of yield face in the π -plane, that is,

$$t = \frac{q}{2} \left[1 + \frac{1}{K} - \left(1 - \frac{1}{K} \right) \left(\frac{r}{q} \right)^3 \right] \quad (7)$$

where K denotes the ratio of the triaxial tensile yield stress to triaxial compression yield stress, known as the flow stress ratio which controls the dependence of yield face on the intermediate principal stress. For the extended Drucker-Prager linear model, the following is deduced:

$$K = \frac{3}{3 + \tan \beta} \quad (8)$$

The experimental data in Fig. 3 can be fitted by a linear equation by the least squares method, and the intercept is set as 0, which represents the non-viscous characteristic of NMG. And then the extended Drucker-Prager linear model parameters are obtained, as shown in Table 1.

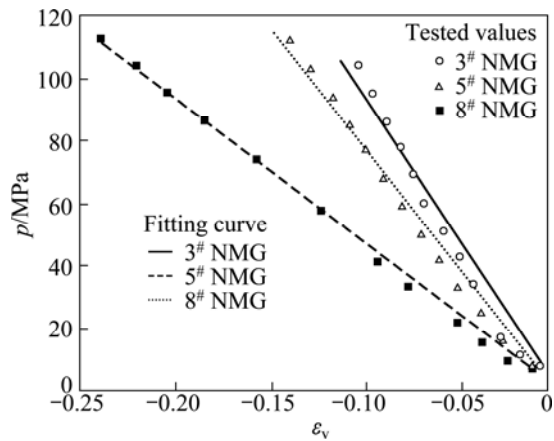


Fig. 3 ε_v - p curves of NMG

Table 1 Extended Drucker-Prager linear model parameters of NMG

NMG No.	Linear fitting equation	$\beta/(\circ)$	K
3#	$q=0.51p, R^2=0.99$	26.8	0.86
5#	$q=0.61p, R^2=0.98$	31.4	0.83
8#	$q=0.67p, R^2=0.97$	33.8	0.82

The GS remarkably engenders unrecoverable plastic deformation when bearing load, which primarily results from dislocation, squeeze close, variation of relative position as well as fracture of the SGM. The relation curves between the volume strain ε_v and the average principal stress p of NMG are obtained through experiments, as shown in Fig. 3.

When the NMGs undergo a triaxial compression stress state, that is, $\sigma_1 > \sigma_2 = \sigma_3$, the volume strain ε_v and the average principal stress p is expressed as

$$p = \lambda \varepsilon_v = q / \tan \beta \tag{9}$$

where λ denotes the volume compression amount.

The volume compression ratio curve reflects the volume varying process of the NMG during the loading process, with the manifestation that the volume changes under high pressure are fitted by the linear function more precisely, and then the constitutive equation of NMG is obtained (see Table 2).

Table 2 Parameter of constitutive equation for NMG

NMG No.	Linear fitting equation	λ/MPa
3#	$p=-926.86\varepsilon_v, R^2=0.97$	926.86
5#	$p=-770.44\varepsilon_v, R^2=0.98$	770.44
8#	$p=-465.62\varepsilon_v, R^2=0.99$	465.62

2.2 Friction strength measurement on SGM

SGM is a collection of scattered and fragmentary

particles. In addition, the linkages between the particles are relatively weak, whose strength does not directly depend on the strength of the particles themselves, but primarily on the interaction between the particles. Shear stress has a greater impact on the destruction of GS, that is to say, shear strength is chiefly comprised of cohesion and friction between the particles. In this work, the sliding and occlusion effect of the particles are all brought into friction strength analysis of GS. The self-designed friction strength testing device of SGM under high pressure is shown in Fig. 4. The relation curve between normal stress σ and shear stress τ of NMG is derived through experiment, as shown in Fig. 5.

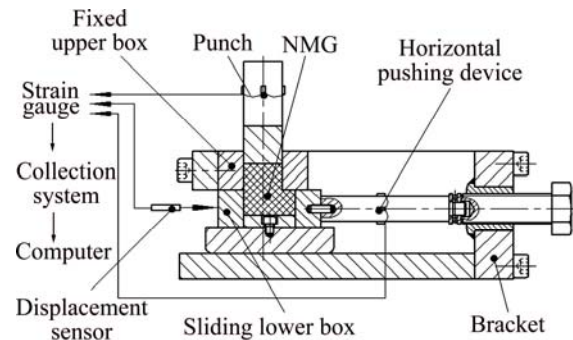


Fig. 4 Friction strength testing device of NMG

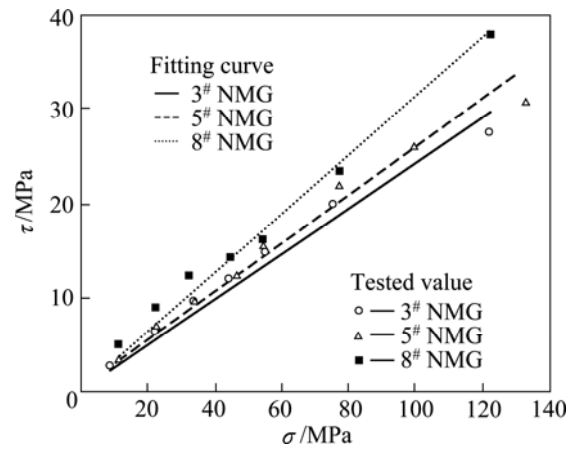


Fig. 5 Relation curve between normal stress σ and shear stress τ of NMG

Internal friction exists between the granules, with the characteristics that the shear strength increased coincidentally with the increase of the normal pressure, which serves as a significant difference from that of metal materials, expressed by pressure hardness, and the change relationship is fitted precisely by linear equations. Simultaneously, the shear strength increases with particle size expansion as well. Test results prove consistent with the Mohr-Coulomb yield criteria, that is,

$$\tau = c - \sigma \tan \phi \tag{10}$$

where ϕ is internal friction angle of the granules, c is

viscosity force of material, $c=0$ for non-viscous granules.

Mohr-Coulomb yield criterion was proposed based on the Mohr circle of the stress state as the material, whose failure line is a straight line tangent to Mohr circle. That is, it is assumed that the material destruction has nothing to do with the intermediate principal stress σ_2 by the Mohr-Coulomb yield criterion. At the same time, it is indicated that not only the maximum shear stress but also the most dangerous combinations of $\tau-\sigma$ on a plane serve as the overriding reason for material failure. The cohesive force equals 0 when the stress state of NMG is $0 > \sigma_1 = \sigma_2 > \sigma_3$.

$$(\sigma_1 - \sigma_3) - (\sigma_1 + \sigma_3) \sin \phi = 0 \tag{11}$$

The extended Drucker-Prager linear model could be expressed by principle stress:

$$(\sigma_1 - \sigma_3) - \frac{\tan \beta}{2 + \frac{1}{3} \tan \beta} (\sigma_1 + \sigma_3) = 0 \tag{12}$$

Combining Eq. (11) with Eq. (12) as

$$\tan \beta = \frac{6 \sin \phi}{3 - \sin \phi} \tag{13}$$

Eq. (13) was substituted into Eq. (8) as

$$K = \frac{3 - \sin \phi}{3 + \sin \phi} \tag{14}$$

$0.778 \leq K \leq 1.0$ is required in order to ensure the yield surface convex in the extended Drucker-Prager linear model. Consequently, $\phi \leq 22^\circ$ is derived by Eq. (14). Therefore, for materials of smaller friction angle, the parameters of the Mohr-Coulomb model and the extended linear model of Drucker-Prager are matched by Eq. (13) [18].

The experimental data in Fig. 5 are fitted by a linear equation by the least squares method, and the intercept was set as 0. Mohr-Coulomb model parameters are available in Table 3. The friction angle β in Table 3 is the solution value of Eq. (13), which has verified the feasibility of the test values.

Table 3 Mohr-Coulomb model parameter of NMG

NMG No.	Linear fitting equation	$\phi/(^\circ)$	$\beta/(^\circ)$
3 [#]	$\tau=0.24\sigma, R^2=0.97$	13.5	26.9
5 [#]	$\tau=0.26\sigma, R^2=0.96$	14.4	28.8
8 [#]	$\tau=0.31\sigma, R^2=0.98$	17.2	33.3

2.3 Test of friction coefficient between NMG and sheet metal

By changing the sliding lower box of the friction coefficient test device (Fig. 4), the sliding friction coefficient between the sheet metal and NMG is tested, known as the largest outside friction coefficient,

expressed by f_w . The curves of the largest outside friction coefficient varying with the pressure for NMG in different sizes are obtained through experiments, as shown in Fig. 6. Friction coefficient f_w is gradually enhanced with the increase of the positive pressure and is fitted precisely by power exponent function when $\sigma < 75$ MPa. Nevertheless, f_w is tending to be a fixed value with the change of positive pressure when $\sigma > 75$ MPa. Friction coefficient f_w increases with the decrease of particle size under the same positive pressure level. The relation between sliding friction coefficient f_w and pressure σ is fitted according to test data curve (see Table 4).

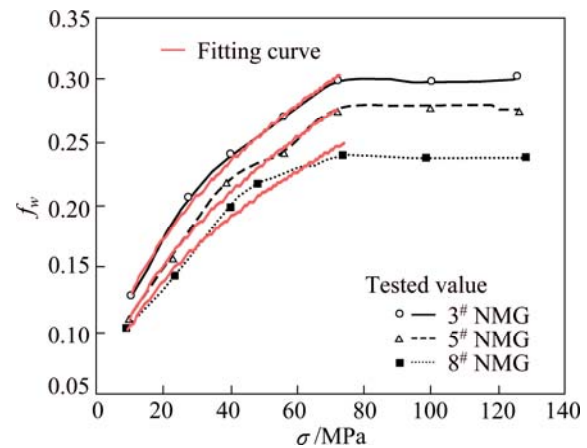


Fig. 6 Outside friction coefficient f_w curves of NMG

Table 4 Sliding friction coefficient of NMG

NMG No.	Fitting equation	
	$0 < \sigma < 75 \text{MPa}$	$75 \text{MPa} \leq \sigma < 140 \text{MPa}$
3 [#]	$f_w=0.047\sigma^{0.43}, R^2=0.996$	$f_w=0.30$
5 [#]	$f_w=0.038\sigma^{0.47}, R^2=0.993$	$f_w=0.28$
8 [#]	$f_w=0.037\sigma^{0.44}, R^2=0.984$	$f_w=0.24$

3 Finite element numerical simulation and analysis

3.1 Establishment of finite element model

A finite element analysis model which consists of two deformable bodies of the sheet metal and SGM is developed. The extended Drucker-Prager linear model is capable of reflecting the pressure hardness of the material. In addition, the yield strength is bound up with confining pressure, and the compressive yield strength is much larger than the tensile yield strength, which is suitable for the friction materials such as scattered mitochondria materials.

Non-associated flow rule for granular materials is commonly employed in the $p-t$ plane of the extended Drucker-Prager linear model, which demonstrates that plastic flow direction on the π -plane is perpendicular to the yield surface [18], as shown in Fig. 7.

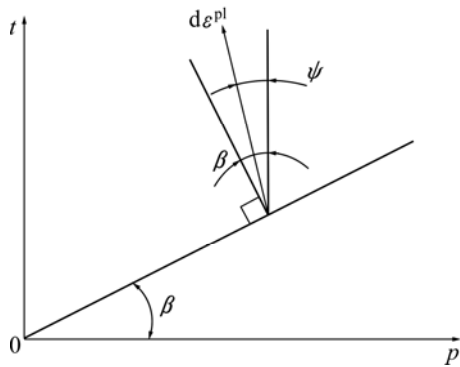


Fig. 7 Fluxion geometric description of linear model on $p-t$ plane

Among them, ψ represents the dilation angle on the $p-t$ plane, the linear model is expressed as

$$G = t - p \tan \psi \tag{15}$$

where G denotes the plastic flow potential.

Non-associated flow rule is usually adopted to simulating granular material, i.e. $\psi < \beta$. KONG et al [19] have recently proved non-associated flow rule dilatancy angle $\psi = \beta/2$ on the basis of the theoretical analysis and the ultimate finite element method. The material model parameters of the NMG are set according to the performance test as well as the extended Drucker-Prager linear model, as shown in Table 5. For the NMG, with the application of the adaptive grid technology, the 8-node linear hexahedral elements with reduced integration C3D8R are employed.

Table 5 Simulation parameters of NMG

NMG No.	$\beta/(^\circ)$	K	$\psi/(^\circ)$	Drucker-Prager hardening
3 [#]	26.8	0.86	13.4	$p=926.86\epsilon_v$
5 [#]	31.4	0.83	15.7	$p=770.44\epsilon_v$
8 [#]	33.8	0.82	16.9	$p=465.62\epsilon_v$

The contact friction between the NMG medium and the sheet metal exhibits outstanding influence on the sheet deformation. Therefore, without precise frictional contact establishment in the simulation, accurate reflection of the forming characteristics cannot be obtained. The penalty function method is adopted in the numerical model to achieve smooth sliding between the contact surfaces, with the surface–surface contact as contact type. The friction coefficient between the SGM and the sheet metal, related to the contact pressure, is set according to Table 4.

The performance of the materials in the 0Cr18Ni9Ti sheet was examined through the application of the INSPEKT Table 100 kN electronic universal testing machine. Specimen, taken from the sheet to be tested, was made by adopting UHP water cutting method. The

angles between the length and the sheet rolling direction were 0, 45° and 90°, respectively, and the dimensional tolerance was no greater than 0.02 mm (see Fig. 8). Sheet material performance parameters (see Table 6) were obtained from the test in which the strain rate was set as 0.0004 s^{-1} with the constant strain rate control mode.

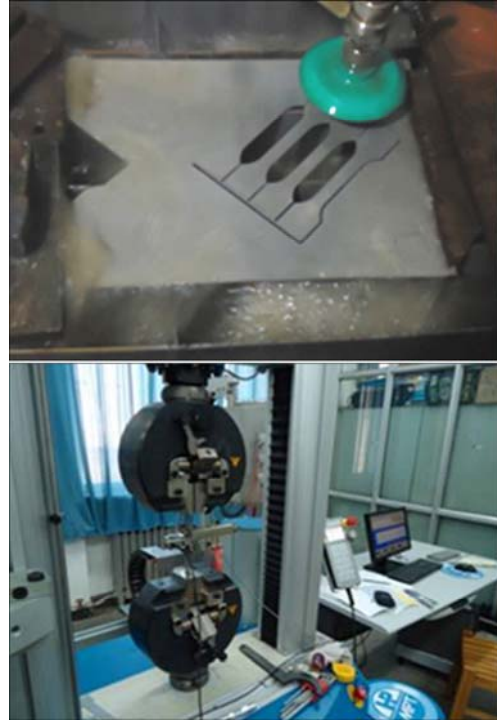


Fig. 8 Sample processing and tensile test

Table 6 Material properties of 0Cr18Ni9Ti steel

Tensile direction	Yield strength/MPa	Ultimate tensile strength/MPa	Total elongation	Plastic strain ratio, r	Strain hardening coefficient, n
0°	266.3	747.5	59.91	0.934	0.425
45°	255.6	704.5	63.49	1.245	0.401
90°	262.3	713.3	65.16	0.817	0.402
Average	261.4	721.7	62.86	1.060	0.409

The true stress–strain curve of sheet is shown in Fig. 9, and it can be fitted by linear equation, namely,

$$\sigma = \sigma_0 + k\epsilon \tag{16}$$

where σ is the true stress, ϵ is the true strain, σ_0 is the initial yield stress, and k is the strength coefficient. The linear equation fitting parameters are shown in Table 7.

In order to more accurately describe the bending effect as well as the thickness direction stress and strain characteristics during the sheet deformation process, seven integration points were set along the thickness direction. The contact friction coefficient between the sheet metal and the die was set to be 0.05. The 1/4

analysis model was established as follows: the punch, the female die, the pressure head and the floating triangle, etc. were all treated as rigid bodies, and the blank holder gap (BHG), back pressure and other parameters were set in accordance with the actual working condition, as shown in Fig. 10. The study and analysis of the relevant process parameters in the deep drawing forming for the parabolic parts lay a reference for the formulation of the mold design and process route.

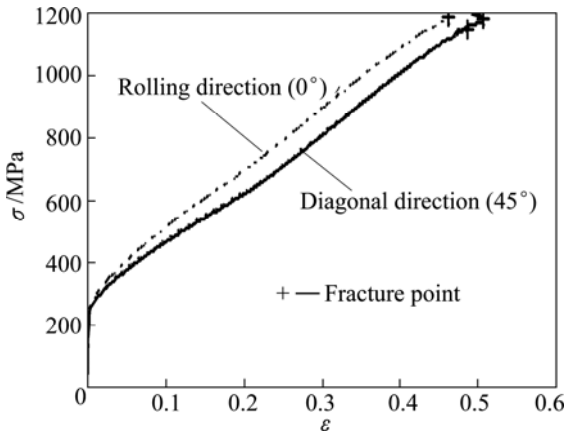


Fig. 9 True stress—strain curves for 0Cr18Ni9Ti steel

Table 7 Parameters fitted by linear equation

Tensile direction/(°)	ϵ	σ_0/MPa	k/MPa	R^2
0	0.004–0.462	266.2	2065.9	0.993
45	0.004–0.485	260.4	1863.9	0.997
90	0.004–0.508	260.4	1850.3	0.998
Average		261.9	1936.0	

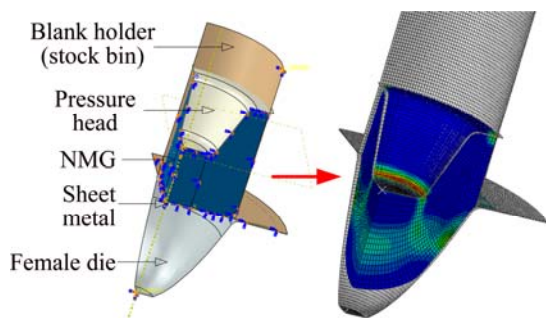


Fig. 10 Numerical simulation model

3.2 Analysis of finite element results

Sheet metal forming test was conducted with the deep parabolic part as typical object. The shape and dimensions of the part are shown in Fig. 11. The relative height of parabolic parts $h/d=0.685$ (relative height, namely a ratio of the forming height and the opening diameter) and plate thickness $\delta_0=0.8$ mm wherein 2 to 4 working steps are generally required to make use of the ordinary deep drawing process.

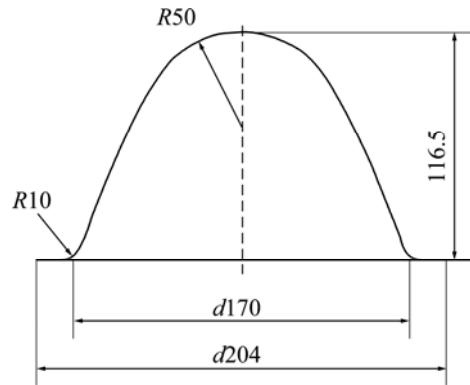


Fig. 11 Parabolic part of sheet metal forming test (unit: mm)

The controlling method of BHG was adopted, namely, the BHG was kept constant in the drawing process. This work assumes that $BHG=1.12\delta_0$, and the parameters of 5# NGM was given, and the workpiece thickness distribution was gained (see Fig. 12).

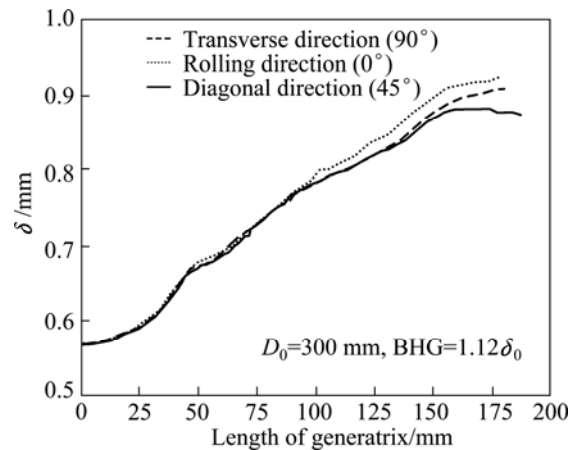


Fig. 12 Workpiece thickness distribution by numerical simulation

The results show that the wall thickness distribution reflects anisotropic, the lug is generated at the flange region that is 45° with the rolling direction, but the thickness difference is not significant. The diameter of initial blank was given as $D_0=275$ mm. The flange diameter of the formed workpiece is bigger and closest to the target workpiece. Therefore, in the following finite element simulation analysis the initial blank diameter is assumed to be $D_0=275$ mm. Wherein the BHG is set as $1.12\delta_0$ by finite element simulation. The medium parameters of different particle sizes are given afterwards, the relation curve between the head pressure F and the stroke S is calculated in Fig. 13 and the distribution curve of thickness δ of the workpiece along the radius r is shown in Fig. 14.

Figure 13 spreads the discrepancy of volume compression modulus for different NMG which resulted

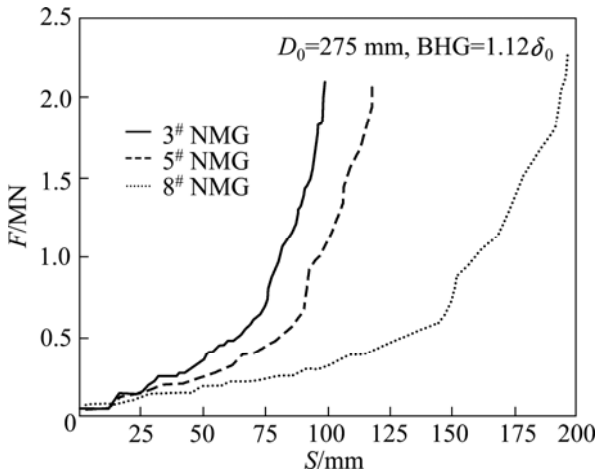


Fig. 13 Loading curve for different size media

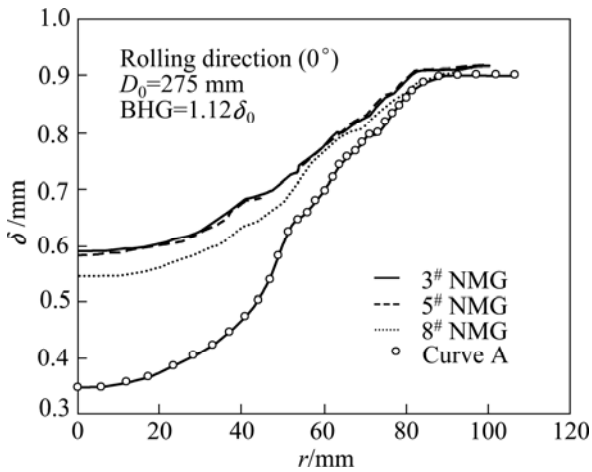


Fig. 14 Simulated distribution curves of workpiece thickness for different size media

in considerable volume compression as well as significant differences in loading curve of 8[#] NMG particles when forming. However, the forming loads of the three kinds of medium are basically identical and the maximum forming load is close to 2200 kN.

Figure 14 shows that the difference in NMG has a certain impact on the wall thickness distribution, but the wall thickness distribution law is relatively approximate and the thinnest wall thickness entirely occurs in the bottom center area. The most significant friction emerges between the smaller size of 3[#] NMG and sheet surface. Simultaneously, the thinnest wall thickness is 0.59 mm and the maximum wall thickness discrepancy is 0.31 mm. Nevertheless, for the application of 8[#] NMG medium, the above values are respectively 0.54 mm and 0.36 mm as well. The wall thickness distribution between 5[#] NMG and 3[#] NMG is comparatively resemble. The wall thickness distribution curve A in Fig. 14 after die fitability and the thinnest wall thickness of about 0.35

mm was obtained to remove particulate medium under the circumstances of uniform load merely given in the sheet loading area. It is thus clear that, the formability as well as the drawing limit of the sheet are significantly improved on account of the action of tangential friction between SGM and the sheet surface which incarnates an major advantage features of the process.

Finite element simulation employed the 5[#] NMG granular media parameters and three BHG samples with range of $1.06\delta_0$ – $1.19\delta_0$ were selected. Hence, the workpiece thickness curves under different BHGs (see Fig. 15) are output.

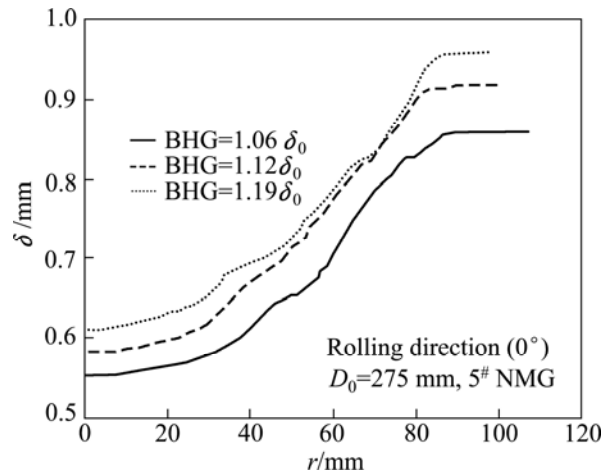


Fig. 15 Workpiece thickness curves under different BHGs

It can be seen from Fig. 15 that the BHG variations have a greater impact on the thickness distribution of the workpiece. As the BHG increases, the thinning of the bottom central zone slows down while the thickening of the flange zone enhances, but at the same time the differences in wall thickness of the whole work-piece are fundamentally identical. Smaller BHG will give rise to extravagant thinning in the bottom central zone, while greater BHG will lead to wrinkles and warps on the flange zone, thereby impacting the deep drawing quality of the sheet metal.

In summary, the numerical simulation shows that when 3[#] or 5[#] NMG medium with smaller particle size is applied to drawing the work-piece, not only the volume compression ratio but also the wall thickness discrepancy is less. Nevertheless, it is not ample to account for the smaller size of particles more appropriate as pressure-transfer medium for sheet metal forming. In the actual applications of the process, if the BHG is greater than the SGM size, parts of granules are possible to enter the sheet blank holding region, which impedes the deformation and flow of the sheet and affects the forming quality as well. However, in the numerical simulation, the assumed GS gives priority to the

compressive stress-based continuum, which cannot manifest the phenomenon above. Thus, the choice and determination of the SGM and BHG are promised to be in accordance with the demand for the practical working conditions. In this work, the medium 5[#] NMG was initially selected and the BHG is $1.12\delta_0$, namely, the gap between the sheet surface and the blank holder is less than the minimum size of the granule medium. The required maximum forming force is 2070 kN obtained by numerical simulation, and the wall thickness distribution contours for the formed workpiece is received, as shown in Fig. 16.

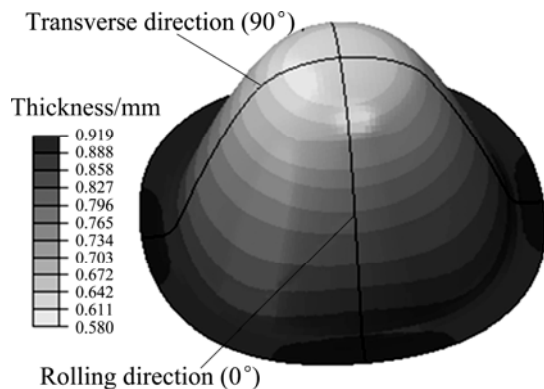


Fig. 16 Wall thickness distribution contours for formed workpiece

4 Study of process experiment

YX-300/500A double-action hydraulic press was selected as the pressure equipment, and the data signals of pressure and displacement of sliders of both inside and outside were collected. The part was made of 0Cr18Ni9Ti sheet, with initial plate thickness $\delta_0=0.8$ mm, diameter slab $d=275$ mm. The BHG was set and adjusted through rigid gaskets. The U.S. ARROW337 lubricant was employed for the use of plate and mold lubrication. Force-transfer medium with NMG gets it suitable for storage bin seal which is so simple that seal is guaranteed by the gap of the indenter and the storage bin wall.

In this process test, NMG with different particle sizes was changed in the first place and the BHG was determined as $1.12\delta_0$ (0.9 mm). Tests show that when 5[#] NMG was used, the load curve and simulation curve were fundamentally identical, as shown in Fig. 17.

Through the tests, workpieces of different forming stages were obtained and their contour shapes were measured, as shown in Fig. 18. Analysis showed that in the forming process, the shape of the free deformation zone was precisely fitted by a spherical cap surface, which was basically the same as that gained by

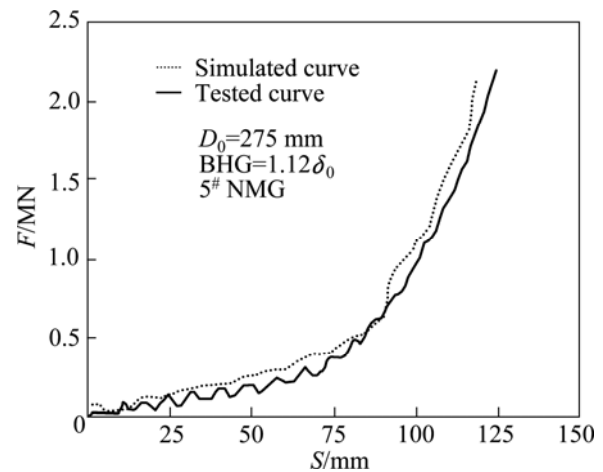


Fig. 17 Comparison of loading curve between test and numerical simulation

numerical simulation. Radius R gradually decreased with the deformation proceeding and finally fitted the bottom of the female die.

In the forming process, the coupled deformation between sheet and SGM took place wherein SGM was clad on the surface of the deformed sheet from beginning to end. As a result of the combined effect of tangential friction between SGM and the sheet as well as internal pressure pull inflation, the free deformation zone gradually reduces as forming increases, and gradually fits the female die. In this work, the workpiece was cut with wire cut electrical discharge machining, and repeated measurement of wall thickness with a vernier caliper was conducted, then those of numerical simulation were compared using the same process parameters, as shown in Fig. 19.

The free deformation zone in plate center turns out to be the most dangerous area of deep rupture whereby it bears double tensile stress state and gradually becomes thinner with the development of forming. The thinning on the bottom center is 0.57 mm which is slightly smaller than the numerical simulation result 0.58 mm and the die is fully fitted when the forming force $F=2188$ kN, wherein the thickness-direction strain $\epsilon_t \geq -0.147$ and the overall wall thickness difference is not greater than 0.33 mm. The wall thickness distribution of the work-piece turns out to be in good agreement with the actual measured results (see Fig. 19). The numerical model of sheet flexible-die forming process with SGM shows that the material properties are defined by the expanded Drucker-Prager linear model for NMG and the forming process scheme is developed basically by relevant model parameters, which lays a guidance and reference for increasing application of this technology in sheet forming.

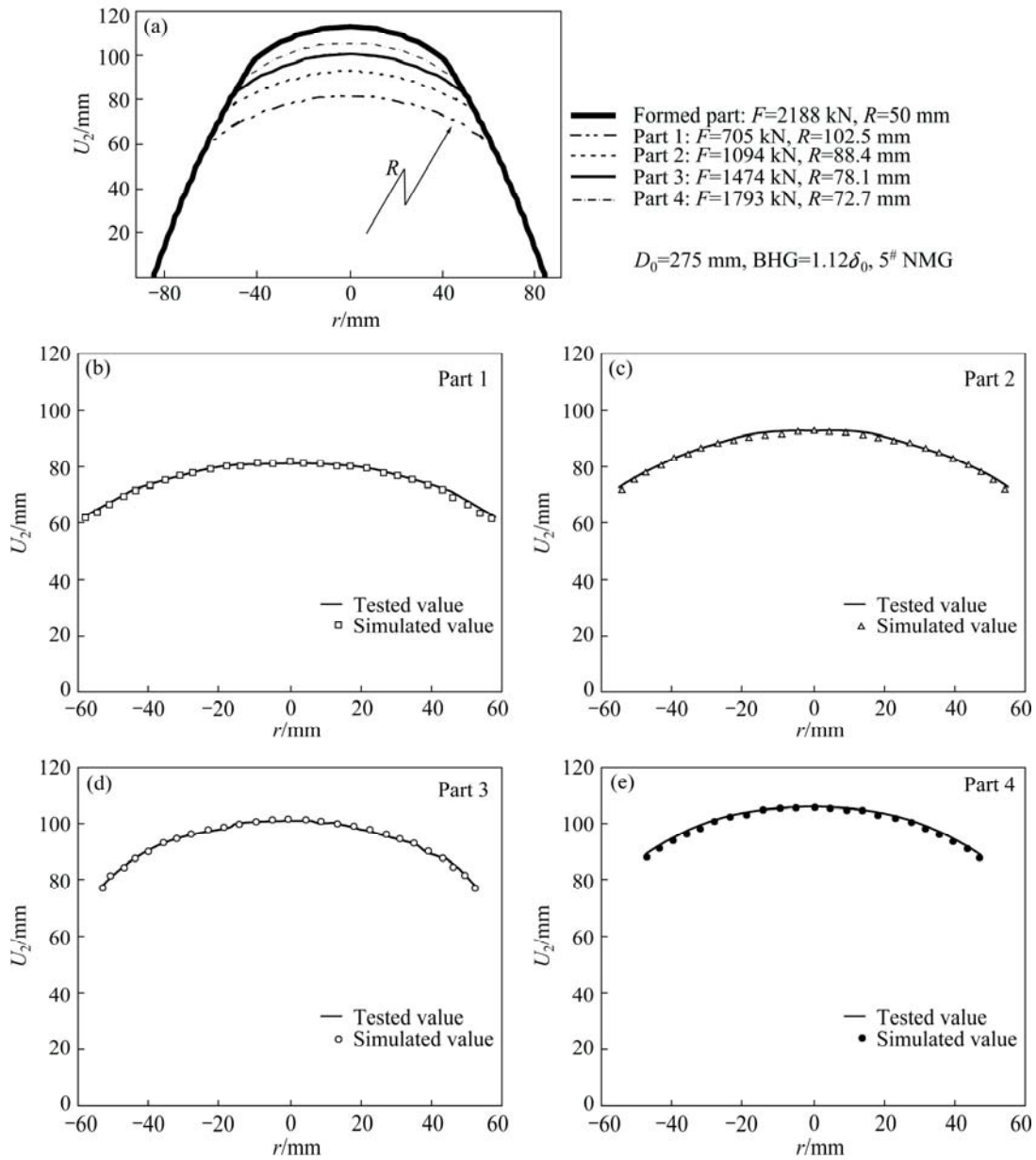


Fig. 18 Different stages of forming workpieces: (a) Profile curves of measured surface for workpieces; (b, c, d, e) Contour comparison of experiment and numerical simulation

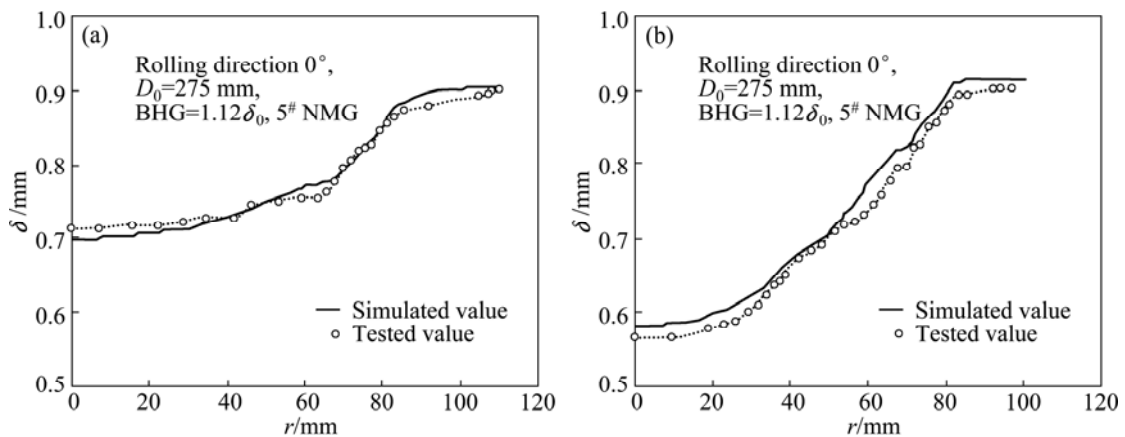


Fig. 19 Comparison of wall thickness distribution curves between experimental and numerical simulation of workpiece: (a) Part1: $F=705$ kN, $U_2=79.2$ mm; (b) Formed part: $F=2188$ kN, $U_2=116.3$ mm

5 Conclusions

1) The material performance test of SGM shows that the stress yield locus of NMG on the p - q plane can be precisely fitted by a linear equation, the volume strain and the average principal stress also have a linear relationship. Furthermore, the shear strength of NMG is enhanced with the normal pressure increasing, with the manifestation of notable pressing-hardness. Test results have an agreement with the Mohr-Coulomb yield criteria and linear relationship is embodied between the shear strength and the normal stress on the surface.

2) The material numerical model of NMG medium was constructed according to the extended Drucker-Prager linear model, the finite element method analysis of forming process was conducted, and the optimal process parameters were initially identified as well. The comparisons between the load curve, the workpiece surface contour, the wall thickness distribution curves of numerical simulation and those of the experimental tests demonstrate that the numerical model is accurate and reliable, thereby it can be applied to laying a basis for the technology schemes.

3) Technology tests and simulation analyses proved that the sheet formability is significantly improved for the extraordinary friction performance manifested by interaction between SGM and the sheet surface. The application of the 5[#] NMG granular media can form complex parabolic parts with uniform thickness, the thickness-direction strain $\varepsilon_z \geq -0.147$, and high surface quality and favorable die fittability. Employment of thermoduric SGM can overcome the sealing and loading problems at high temperatures of general media, which makes it suitable for the pressure forming of high-strength alloy materials with complex shape and low deformability.

References

- [1] LIU Xiao-jin, YAN Wei, GUO Li-wei. Numerical simulation of aluminum-magnesium alloy cup's forming by hydrodynamic deep drawing with double loading paths [J]. The Chinese Journal of Nonferrous Metals, 2008, 18(4): 698–702. (in Chinese)
- [2] WANG Gang, WANG Jian-long, ZHANG Tuo-da, ZHANG Zhi-peng. Quick gas blow forming behavior of AZ31B magnesium alloy sheet [J]. The Chinese Journal of Nonferrous Metals, 2011, 21(9): 2023–2027. (in Chinese)
- [3] CUI Xiao-hui, MO Jian-hua, ZHU Ying. 3D modeling and deformation analysis for electromagnetic sheet forming process [J]. Transactions of Nonferrous Metals Society of China, 2012, 22(1): 164–169.
- [4] LIU Xin, XU Yong-chao, YUAN Shi-jian. Hydro-forming of aluminum alloy complex-shaped components [J]. Transactions of Nonferrous Metals Society of China, 2011, 21(s2): s417–s422.
- [5] LIU Wei, LIU Gang, CUI Xiao-lei, XU Yong-chao, YUAN Shi-jian. Formability influenced by process loading path of double sheet hydroforming [J]. Transactions of Nonferrous Metals Society of China, 2011, 21(s2): s465–s469.
- [6] AHMETOGLU M, JIANG H, KULUKURU S, ALTAN T. Hydroforming of sheet metal using a viscous pressure medium [J]. Journal of Materials Processing Technology, 2004, 146: 97–107.
- [7] WANG Zhong-jin, YI Li. Formability of 6k21-T4 car panel sheet for viscose elastic-plastic flexible-die forming [J]. Journal of Materials Processing Technology, 2008, 201: 408–412.
- [8] HAMA T, HATAKEYAMA T, ASAKAWA M, AMINO H, MAKINOCHI A, FUJIMOTO H, TAKUDA H. Finite-element simulation of the elliptical cup deep drawing process by sheet hydroforming [J]. Finite Elements in Analysis and Design, 2007, 43: 234–246.
- [9] KHANDEPARKAR T, LIEWALD M. Hydromechanical deep drawing of cups with stepped geometries [J]. Journal of Materials Processing Technology, 2008, 202: 246–254.
- [10] LANG L, GU G, LI T, ZHOU X. Numerical and experimental confirmation of the calibration stage's effect in multi-operation sheet hydroforming using poor-formability materials [J]. Journal of Materials Processing Technology, 2008, 201: 97–100.
- [11] WANG Hui-ting, ZHANG Jing, GAO Lin, SHEN Xiao-hui. Hydrodynamic deep drawing process with hybrid blank holder [J]. Journal of Mechanical Engineering, 2011, 47(16): 73–78. (in Chinese)
- [12] WANG Hui-ting, GAO Lin, SHEN Xiao-hui, CHEN Ming-he. Hydrodynamic deep drawing process with hybrid blank holder [J]. The Chinese Journal of Nonferrous Metals. 2010, 20(5): 840–845. (in Chinese)
- [13] LIU Jiang-guang, WANG Zhong-jin. Prediction of wrinkling and fracturing in viscous pressure forming (VPF) by using the coupled deformation sectional finite element method [J]. Computational Materials Science, 2010, 48: 381–389.
- [14] FU M W, LI H, LU J, LU S Q. Numerical study on the deformation behaviors of the flexible die forming by using viscoplastic pressure-carrying medium [J]. Computational Materials Science, 2009, 46: 1058–1068.
- [15] ZHAO Chang-cai, CAO Miao-yan, XIAO Hong, DONG Guo-jiang, HAO Hai-bin. Solid granular medium drawing process parameters of magnesium alloy sheet [J]. The Chinese Journal of Nonferrous Metals. 2012, 22(4): 991–999. (in Chinese)
- [16] CAO Miao-yan, ZHAO Chang-cai, DONG Guo-jiang. Numerical simulation on granules medium drawing process parameters of magnesium alloy sheet [J]. The Chinese Journal of Nonferrous Metals, 2012, 22(11): 2992–2999. (in Chinese)
- [17] DONG Guo-jiang, ZHAO Chang-cai. Study on the forming of Box-shaped parts based on solid granule medium forming [J]. Journal of Mechanical Engineering, 2012, 48(20): 45–52. (in Chinese)
- [18] LI Guang-xin. Advanced soil mechanics [M]. Beijing: Tsinghua University Press, 2004. (in Chinese)
- [19] KONG Wei-xue, RUI Yong-qin, DONG Bao-di. Determination of dilatancy angle for geomaterials under non-associated flow rule [J]. Rock and Soil Mechanics, 2009, 30(11): 3278–3282. (in Chinese)

基于固体颗粒介质的板材软模成形工艺

董国疆¹, 赵长财¹, 曹秒艳²

1. 燕山大学 先进锻压成形技术与科学教育部重点实验室, 秦皇岛 066004;
2. 燕山大学 冷轧板带装备及工艺国家工程技术研究中心, 秦皇岛 066004

摘要: 选用非金属颗粒(NMG)作为研究对象, 通过体积压缩试验和 NMG 在高应力水平下的物理性能试验, 得到 NMG 体积压缩曲线和扩展的 Drucker-Prager 线性模型参数; 通过摩擦强度试验, 得到 NMG 的 Mohr-Coulomb 模型参数, 并与扩展的 Drucker-Prager 线性模型参数比对基本吻合; 测定了 NMG 与板材在不同正压力下的摩擦因数曲线。以材料性能试验为基础, 对基于固体颗粒介质的板材软模成形工艺进行数值分析; 设计制造固体颗粒介质板材成形试验模具, 成功制出抛物线形零件。结果表明: 固体颗粒介质与板材表面作用所表现出的显著摩擦性能, 可以极大地发挥板料的成形性能; 其工艺控制简便, 模具结构简单; 成形工件具有表面质量好、贴模性好、精度高等优点, 为板材的加工和制备提供了新的方法和手段。

关键词: 固体颗粒介质成形; 拉深; 板材; 有限元模拟

(Edited by Xiang-qun LI)